Numerical and Modeling Issues for Optimization of Flow Control Devices

Régis Duvigneau, Jérémie Labroquère, Emmanuel Guilmineau

50th 3AF International Conference
on Applied Aerodynamics
29-30 March – 01 April 2015, Toulouse - France

FP12-2015-duvigneau

NUMERICAL AND MODELING ISSUES FOR OPTIMIZATION OF FLOW CONTROL DEVICES

R. Duvigneau[1], **J. Labroquère**[1], **E. Guilmineau**[2]

[1] *INRIA Sophia-Antipolis, Acumes Team, 2004 route des lucioles, 06902 Sophia-Antipolis, France*
Email: Regis.Duvigneau@inria.fr, Jeremie.Labroquere@inria.fr

[2] *LHEAA, CNRS UMR6598, Ecole Centrale de Nantes, 1 rue de la Noë 44321 Nantes, France*
Email: Emmanuel.Guilmineau@ec-nantes.fr

INTRODUCTION

Active flow control has been a growing research area for the last decades, since this approach demonstrated its ability to improve aerodynamic performance [6], for a large range of applications. It is especially appealing in case of separated flows, for which natural instability phenomena can be efficiently exploited to manipulate flow characteristics using periodic flow excitation.
In this context, a major difficulty is related to the choice of actuation parameters, such as excitation frequency, amplitude, location, to obtain the expected flow response. In cases implying a single isolated actuator, it is quite easy to carry out an experimental or numerical study to determine efficient control parameters. However, in the perspective of industrial applications based on hundreds of actuators, this task is far from being straightforward and the use of an automated optimization strategy is thus proposed, in the spirit of previous works [3, 4].
While optimization algorithms are now commonly employed in aerodynamics for shape optimization purpose, their use in the context of control devices yields new issues, which are detailed in the present study. In particular, we aim at quantifying the impact of the numerical errors (discretization, convergence) and modeling uncertainties (turbulence closure) on the optimization procedure. The choice of the optimization parameters is also explored. Different test-cases and flow solvers are considered in this study, e.g. NACA airfoil, backward facing step, 25° ramp.

1. FLOW CONTROL: PRINCIPLES AND ISSUES

Active flow control consists in exploiting natural flow instability, by the use of an actuator, to obtain some desired effects with an energy expense as small as possible.
It has been shown, in particular during the CFD-VAL Workshop [11], that the prediction of actuator-induced flows is still tedious, because of the difficulty to model the flow in the vicinity of the actuator and in the separated regions. Even if Large Eddy Simulation (LES) methods usually outclass Reynolds-Averaged Navier-Stokes (RANS) models for such problems, LES methods are still unable to predict actuated flows in a computational time that would be reasonable in an industrial context. In a recent study [7], it has been found that RANS models are not able to predict the correct characteristics of the separation, but some of them are able to identify the best actuation frequency, to reduce the separation length. This encouraging result indicates that RANS models could possibly be used in a design phase to select control parameters. Therefore, we propose in the current work a similar study, in which a full optimization of actuation parameters is performed, for a set of RANS models. The objective is to assess the ability of RANS models to be used in an optimization framework for active flow control.

In the context of the automated optimization, the computational time related to the simulation of unsteady flows is also important, if one wants the optimization time to remain reasonable. We underline that the evaluation of the cost functional is subject to the convergence of unsteady quantities towards their time-averaged values. On the one hand, obtain an accurate time-averaged value could be computationally expensive. On the other hand, reduce the time averaging process will produce noisy cost functional estimations. Therefore, our second objective is to explore the capability of new optimization strategies, based on statistical learning, to account for truncated unsteady simulations and noisy cost functional estimations in a rigorous framework.

The choice of the actuation parameters to optimize is obviously critical. Depending on the test-case,

some parameters could have a more significant impact on the control efficiency than others, but an *a priori* choice is sometimes tedious. We finally illustrate the importance of the parameters choice to obtain a fruitful optimization search.

2. SIMULATION METHODS

2.1 Incompressible flow model

The solver ISIS-CFD, available as a part of the FINE^{TM}/Marine computing suite, is an incompressible unsteady Reynolds-averaged Navier-Stokes (URANS) method mainly devoted to marine hydrodynamics. The method features several turbulence models: apart from the classical two-equation k-ϵ and k-ω models, the anisotropic two-equation Explicit Algebraic Reynolds Stress Model (EARSM), as well as Reynolds Stress Transport Models, are available [5]. All models are available with wall-function or low-Reynolds near wall formulations. Hybrid LES turbulence models based on Detached Eddy Simulation (DES) are also implemented and have been validated on automotive flows characterized by large separations [8]. The solver is based on the finite volume method to build the spatial discretization of the transport equations. The unstructured discretization is face-based. An anisotropic automatic grid refinement procedure has been developed which is controlled by various flow-related criteria [13]. Parallelization is based on domain decomposition. The automatic grid refinement procedure is fully parallelized with a dynamic load balancing working transparently.

2.2 Compressible flow model

The compressible flow analysis is performed using the NUM3SIS platform. The Favre-averaged Navier-Stokes equations are solved on triangular or tetrahedral grids using a mixed finite-volume / finite-element approach. A high-order spatial accuracy is obtained using a MUSCL state extrapolation technique associated with the HLLC approximate Riemann solver to compute convective fluxes, while a P1-Galerkin approach is employed for viscous fluxes [10]. A second-order implicit dual time-stepping procedure is used for the time integration. Spalart-Allmaras and SST $k-\omega$ turbulence closures are used.

2.3 Actuator model

We consider actuations based on synthetic jets (zero-net mass flux), which are implemented as boundary conditions. the velocity is imposed at the jet boundary and is defined as:

$$\mathbf{U} = U_J A(X) sin(\omega t) \mathbf{d}_J \quad (1)$$

with $A(x)$ a unit profile function, U_J the amplitude, ω the angular frequency with $\omega = 2\pi f_J$ where f_J is the frequency, and $\mathbf{d}_J$ the direction of the jet. In this study, $A(X)$ is a sine squared function.

3. OPTIMIZATION STRATEGY

In the context of turbulent unsteady flows, a major issue for optimization is the computational burden of each simulation. The evaluation of the cost functional gradient using an unsteady adjoint approach is highly complex and the non-linear underlying phenomena may yield multimodality. Furthermore, the evaluations are noisy due to simulation errors (discretization, convergence, etc.). For all these reasons, the use of classical descent methods is tedious. Alternatively, stochastic approaches like genetic algorithms or evolution strategies require too many evaluations to be practically tractable. To address these issues, the use of surrogate models in the framework of statistical learning is a promising approach. In particular, this work is focused on the Efficient Global Optimization (EGO) algorithm.
The EGO is a global optimization algorithm that makes use of a stochastic process to drive the optimization [9]. As a first design of experiment phase (DOE), an initial database covering the bounded search space is generated from simulations. This database contains obviously the cost functional values, but may also gather the error estimated for each evaluation. A Gaussian Process model is then constructed using this database, which allows to predict the cost function value in terms of expectancy and variance at any point of the search domain. According to these predictions, the most interesting points are selected by maximizing a merit function, e.g. the expected improvement criterion (EI). These new configurations are finally simulated, the corresponding cost functional values and the error estimations being added to the database. This process is repeated until convergence, as illustrated on Fig. 1.

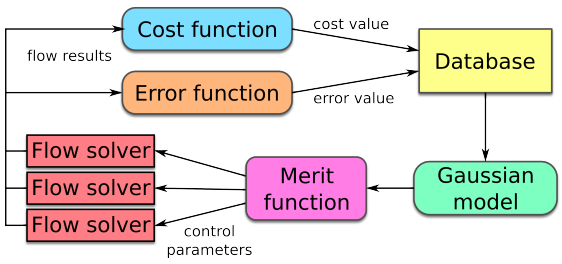

Figure 1: EGO algorithm.

Gaussian Process models (also known as kriging models) belong to response surface methods, that allow to predict a function value f at a given point x, on the basis of a set of observed values $\mathbf{F_N} = \{f_1, f_2, \ldots, f_N\}$ at some points $\mathbf{X_N} = \{x_1, x_2, \ldots, x_N\} \in \mathbb{R}^d$. $\mathbf{F_N}$ is assumed to be one realization of a multivariate Gaussian Process which has a joint Gaussian distribution

$$p(\mathbf{F_N}|\mathbf{X_N}) = \frac{\exp\left(-\frac{1}{2}\mathbf{F_N}^\top C_N^{-1}\mathbf{F_N}\right)}{\sqrt{(2\pi)^N \det(C_N)}}, \qquad (2)$$

for any collection of inputs $\mathbf{X_N}$. C_N is the $N \times N$ covariance matrix, whose elements C_{mn} give the correlation between the function values f_m and f_n obtained at points x_m and x_n. We assume that these values are correlated, since they correspond to underlying physical phenomena. This is expressed in terms of a correlation function k, i.e., $C_{mn} = cov(f_m, f_n) = k(x_m, x_n; \Theta)$ with Θ a set of hyper-parameters that are calibrated on the basis of known points (likelihood maximization principle). The choice of the correlation function k is critical for the model, as it contains all the prior hypotheses, including for example regularity, symmetry, periodicity, etc. The correlation function must *a priori* reflect the characteristics of the output of the computer code. We use here the Matérn class of covariance stationary kernels, which gives a family of correlation functions of different smoothness.

After some calculations based on conditional probabilities, we obtain that the probability density for the function value f_{N+1} at any new point x_{N+1} is:

$$p(f_{N+1}|\mathbf{X_N}, \mathbf{F_N}) \propto \exp\left[-\frac{(f_{N+1} - \hat{f}_{N+1})^2}{2\hat{\sigma}^2_{f_{N+1}}}\right], \qquad (3)$$

where

$$\hat{f}_{N+1} = \mathbf{k_{N+1}}^\top C_N^{-1}\mathbf{F_N}, \qquad (4)$$

$$\hat{\sigma}^2_{f_{N+1}} = \kappa - \mathbf{k_{N+1}}^\top C_N^{-1}\mathbf{k_{N+1}}, \qquad (5)$$

with $\kappa = k(x_{N+1}, x_{N+1}; \Theta)$ and $\mathbf{k_{N+1}} = [k(x_1, x_{N+1}; \Theta), \ldots, k(x_N, x_{N+1}; \Theta)]^\top$. Thus, the probability density for the function value at the new point x_{N+1} is also Gaussian with mean $\hat{f}_{N+1}$ and standard deviation $\hat{\sigma}_{f_{N+1}}$. Therefore, the most likely value at the new point x_{N+1} is $\hat{f}_{N+1}$. This value will be considered as the prediction of the kriging model. The variance $\hat{\sigma}^2_{f_{N+1}}$ can be interpreted as a measure of uncertainty in the value prediction. If the evaluation is known to be noisy, the model can account for the observation noise by modifying the diagonal terms of the covariance matrix, on the basis of the noise variance estimated for each database point [10].

At each step of the optimization procedure, this Gaussian Process model is exploited to determine new points to be simulated. The most popular strategy is the maximization of the Expected Improvement (EI) [9]. The improvement obtained at any point x is defined as $I := \max(f_{\min} - f(x), 0)$, where $f_{\min}$ is the best point found so far. Then, the EI criterion is the expected value of I:

$$EI = \int_0^\infty I \, \frac{1}{\sqrt{2\pi}\hat{\sigma}(x)} \exp - \frac{(f_{min} - I - \hat{f}(x))^2}{2\hat{\sigma}(x)^2} dI. \qquad (6)$$

The maximization of this criterion is achieved numerically, by solving an internal optimization problem using an evolution strategy [2, 10]. In the following sections, this approach is tested on three cases.

4. INFLUENCE OF SIMULATION ERRORS

4.1 Test-case: NACA 0015 Airfoil

We consider the flow around the NACA 0015 airfoil at high angle of attack (18°). The Reynolds number is 5.10^6 and the Mach number 0.15. A synthetic jet is located at 12% of the chord c (slot width 0.5%). The optimization consists in determining the jet frequency to maximize the time-averaged lift, for a fixed jet amplitude equal to the free-stream velocity $U_J = U_\infty$. The non-dimensional frequency $f_J c/U_\infty$ can vary between 0 (no actuation) and 2. The grid counts 153849 nodes, including a refined area around the jet slot. The far-field boundary is located at 100 chords from the airfoil. The distance between the first node and the wall is 1.10^{-5} to fulfill the $y^+ = 1$ criterion. This problem is studied using the compressible flow solver described above, with the SST $k - \omega$ model from Menter.

4.2 Results

The initial database counts five configurations. The corresponding lift coefficient histories show that the convergence towards a periodic flow depends on

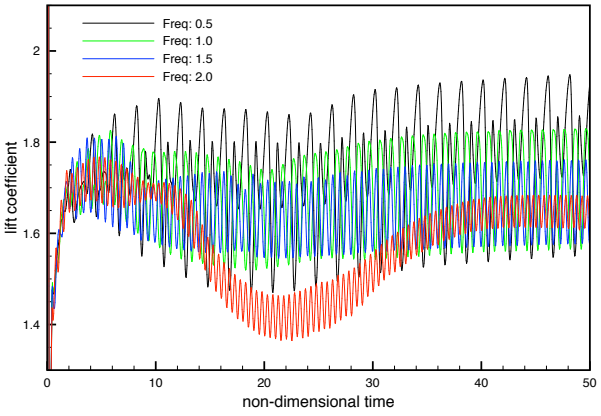

Figure 2: Naca - Time evolution of lift coefficient

the actuation, as illustrated by Fig. 2. Flows with low and high frequency actuation are shown on Figs. 3 and 4.

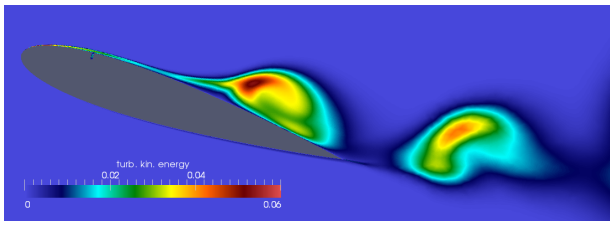

Figure 3: Naca - k field for low frequency actuation.

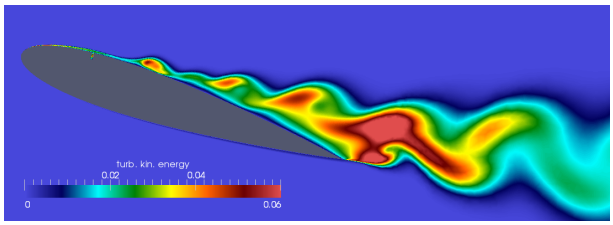

Figure 4: Naca - k field for high frequency actuation.

A naive evaluation of the time-averaged lift coefficient can lead the optimization procedure to failure. If one estimates the performance using only one period after a short time, e.g. around $t = 30$, one obtain the results depicted in Figs. 5 to 7. The Gaussian Process model is represented, in terms of expectancy and variance, and the associated database. The EI criterion that rules the search is also provided. At iteration 0, the initial five points allow to construct a first model. At iteration 3, three new configurations have been added according to the EI criterion, yielding an improved accuracy and a reduction of the variance in the most interesting regions. However, at iteration 5, the model becomes oscillatory and the variance suddenly increases in all regions, which makes further search inefficient. Some experiments have proved that this behavior is due to the presence of noise in the performance estimation.

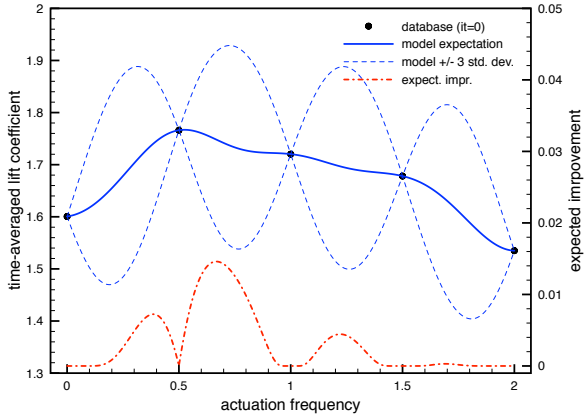

Figure 5: Naca - Kriging model it. 0

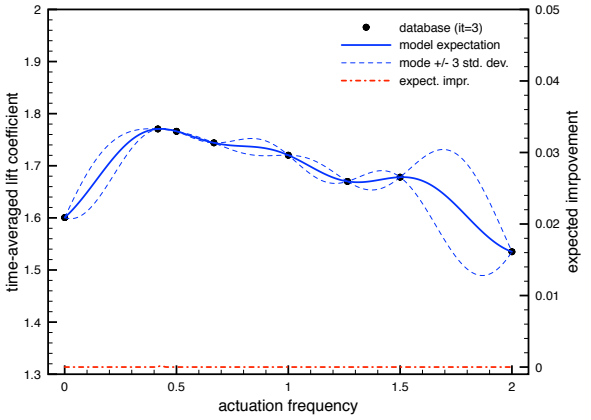

Figure 6: Naca - Kriging model it. 3

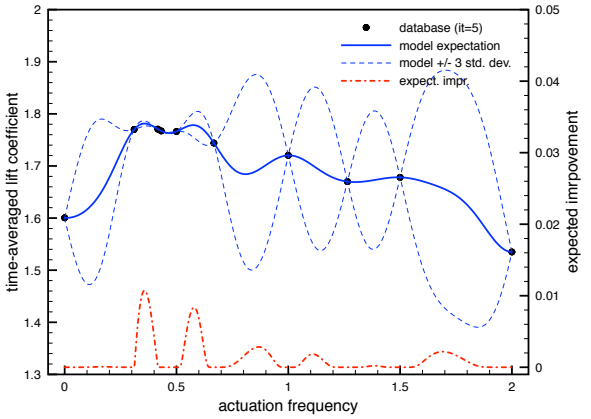

Figure 7: Naca - Kriging model it. 5

To overcome this difficulty, we propose to include an observation noise into the model. In this perspective, a statistical estimation of the performance is carried out. Since a periodic flow of period T is expected, any integration over an interval $T^{(i)}$ of length T can provide an estimate $C_L^{(i)}$ of the time-averaged lift. Therefore, after transient flow has vanished (here $t > 10$), we collect all available time-averaged lift estimates in a set $(C_L^{(i)})_{i=1,\cdots,I}$. Then, the cost functional value and the related observation variance are computed according to this set of estimates using empirical estimators:

$$f = \frac{1}{I}\sum_{i=1}^{I} C_L^{(i)} \quad \sigma^2 = \frac{1}{I-1}\sum_{i=1}^{I}(C_L^{(i)} - f)^2. \qquad (7)$$

This variance estimate is used not only for the construction of the Gaussian Process model, but also to define the ending time of the simulations, in an adaptive strategy. Indeed, we intend to stop any simulation corresponding to a new point x as soon as the corresponding performance seems to be of poor value with respect to the best point found so far x_{min}. On the contrary, we would like to estimate

more accurately the performance if the new point seems to be promising. Therefore, the cost functional value and observation variance in Eq. 7 are computed during the flow simulation at each time step k. The simulation is stopped as soon as the following condition is fulfilled:

$$\hat{f}(x_{min}) - \alpha\hat{\sigma}_f(x_{min}) < f_k(x) - \alpha\sigma_k(x), \quad (8)$$

where α is a numerical parameter (here $\alpha = 3$). The left-hand side represents a performance estimate for the best known point, based on the model accounting for its own variance. The right-hand side represents a performance estimate for the current point, including the observation variance. Note that the observation variance reduces as the simulation proceeds. Moreover, the model variance also reduces during the optimization, yielding progressively a stricter criterion for the simulation.
This approche is illustrated in Figs. 8 to 10. One can observe that the model constructed accounts for observation noise, remains stable, and that simulations are more and more accurate as optimization proceeds. Flow with optimal frequency actuation is shown on Fig. 11.

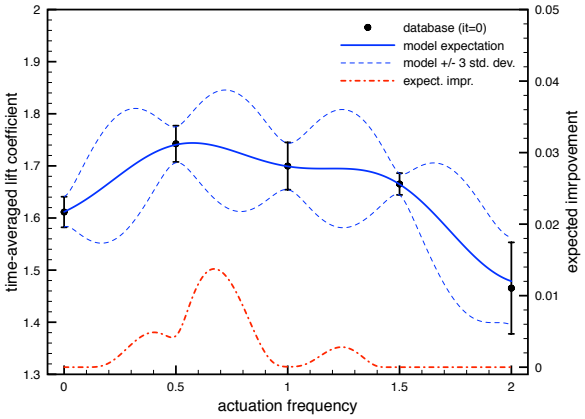

Figure 8: Naca - Kriging model with noise it. 0

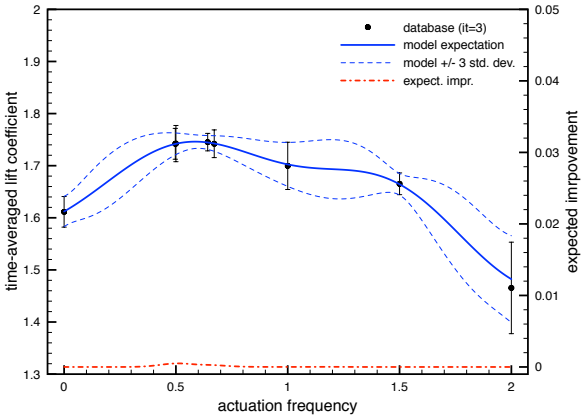

Figure 9: Naca - Kriging model with noise it. 3

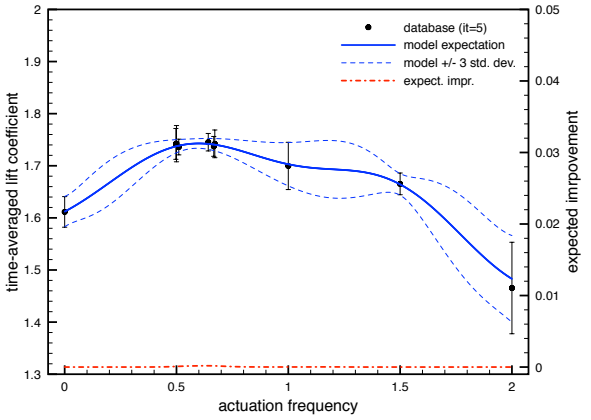

Figure 10: Naca - Kriging model with noise it. 5

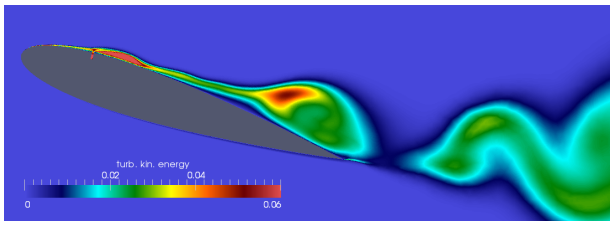

Figure 11: Naca - k field for optimal actuation.

5. INFLUENCE OF TURBULENCE CLOSURE

5.1 Test-case: backward facing step

The test-case proposed here corresponds to the two-dimensional flow over a backwards facing step, in the conditions described in the experiments carried out by Driver & Seegmiller [1]. This problem is studied using the incompressible flow solver described above. The objective of the actuation is the reduction of the separation length. The geometry of the computational domain, including the actuator, is represented on Fig. 12. Computational parameters are set according to the experimental data: $h = 0.0127\,m$, $U_\infty = 44.2\,m/s$, the boundary layer thickness at the inlet is $\delta_{BL} = 0.019\,m$. The Reynolds number based on this reference length is $Re = 5000$. As boundary conditions, we impose at inlet a turbulent velocity profile corresponding to experiments, and a uniform pressure condition at outlet.

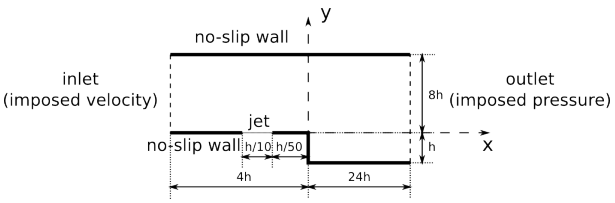

Figure 12: BFS - computational domain.

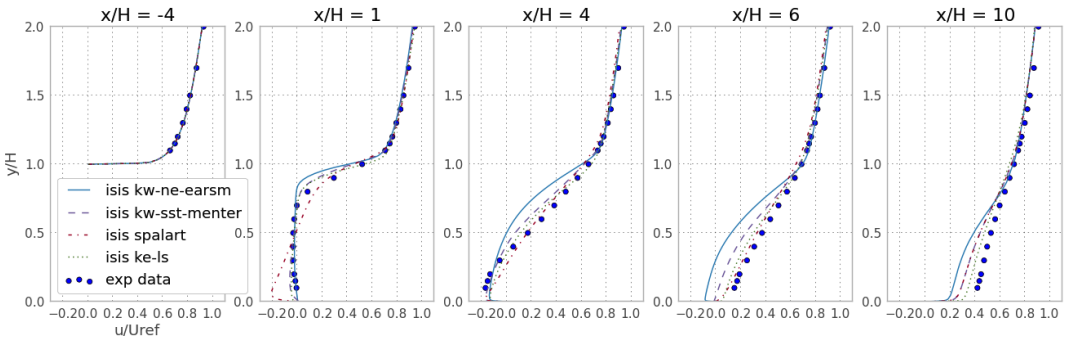

Figure 13: BFS - Comparison of velocity profiles and experimental data.

The mesh generated counts 45805 nodes and includes a refined area between the step and the location $9h$. The distance between the wall and the first node is set to fulfill the condition $y^+ \leq 1$ at all locations, for all closures. The actuator has a width of value h/10 and is introduced at a location very close to the step corner $(h/50)$, generating a vertical suction / blowing actuation.

5.2 Results

Firstly, the characteristics of the flow without actuation are compared for the different turbulence closures considered in this study: Spalart-Allmaras (SA), Launder-Sharma $k-\epsilon$ (KE), SST $k-\omega$ (KW) and algebraic stress model (EASM). In this context, the computations converge towards stationary solutions. A grid convergence study shows that the discretization error is far lower than the modeling error. Velocity profiles are depicted on Fig. (13), for the finest grid, while a comparison of the separation length is provided:

Exp.	SA	KE	SST	EASM
6.26	6.05	5.41	6.37	7.56

Although it deals with a simple test-case, without actuation, turbulence closure plays already a critical role in the flow prediction. In particular, EASM closure overestimates the separation length, while Launder-Sharma $k-\epsilon$ one predicts a too small recirculation region, with respect to experimental measurements. In the next sections, we quantify the effects of the actuation and observe if some common trends can be established, despite of this initial discrepancy.

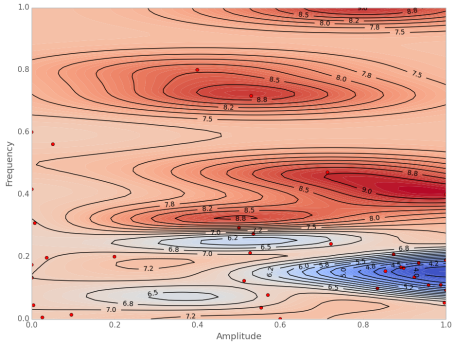

Figure 14: BFS - Cost functional map for SA

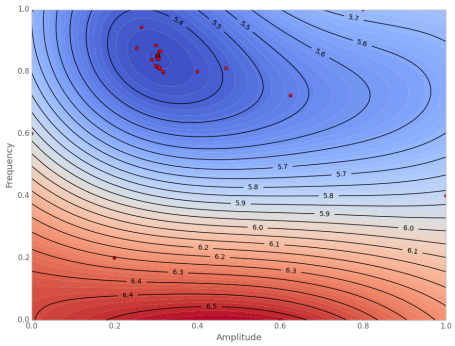

Figure 15: BFS - Cost functional map for SST

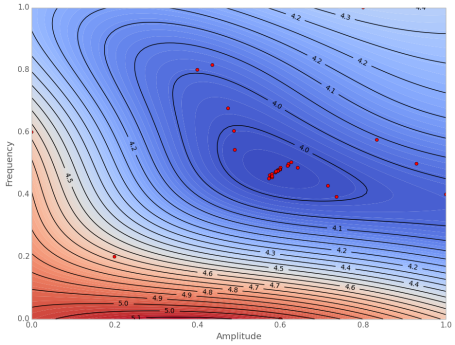

Figure 16: BFS - Cost functional map for KE

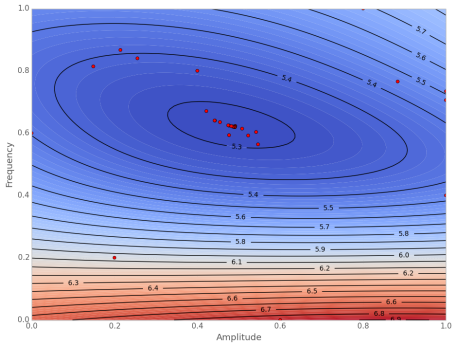

Figure 17: BFS - Cost functional map for EASM

Unsteady computations are carried out until transient effects have vanished. The time step employed is scaled on the actuation frequency, so that all configurations count the same number of time steps per actuation period. For each time step, a reduction of three orders of non-linear residuals is used as stopping criterion. The separation length is computed afterwards, from the time-averaged flow, on the basis of a four-period integration. The parameters of the actuation are the frequency and the amplitude of the jet. They are allowed to vary in the following intervals: $4m/s \leq U_j \leq 50m/s$ and $50Hz \leq f_j \leq 1000Hz$. As explained above, the optimization procedure starts from a DOE phase, composed of only six points, that are selected according to a Latin Hypercube Sampling (LHS). Then, additional points are inserted in the Gaussian Process model, according to the merit function. About ten enrichment steps are performed before convergence of the optimization procedure, corresponding to a total of about 40 simulations per optimization exercise.

Figs. 14 to 17 show the Gaussian process models for the recirculation length, obtained using the different turbulence closures, as well as the configurations computed. As can be seen, the initial set of simulations covers the whole admissible domain, while the next evaluations converge towards the optimal parameters. At first, one can notice that the results based on the Spalart-Allmaras closure exhibit a behavior very different than other cases. In particular, the variations of the separation length with respect to the frequency are very irregular. The examination of the corresponding flows reveals that the Spalart-Allmaras closure predicts for some configurations a massive vortex shedding, which modifies abruptly the time-averaged separation length. The results obtained with the three other closures exhibit some similarities. In particular, only one minimum is identified by the Gaussian Process models. For Launder-Sharma $k-\epsilon$ and EASM closures, it is located in the same region corresponding to medium actuation parameters. For the Menter SST $k-\omega$ closure, the global shape of the response surface is similar, but the minimum corresponds to higher frequency and amplitude. Nevertheless, the precise values of the optimized control parameters are significantly different, as well as the final separation length L_R, as shown in the following table:

	SA	KE	SST	EASM
f_J (Hz)	205	492	828	653
U_J (m/s)	50	31	18	25
L_R/L_{ini}	0.69	0.72	0.84	0.70

Obviously, the "true" optimal actuation value is unknown.

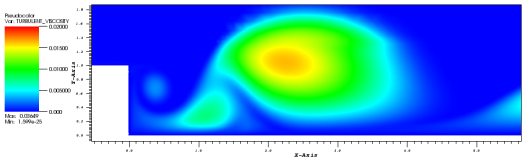

Figure 18: BFS - Optimal μ_t field for SA

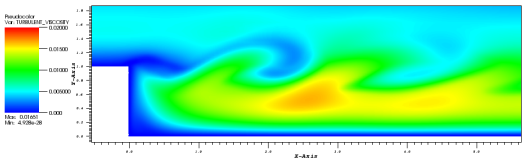

Figure 19: BFS - Optimal μ_t field for SST

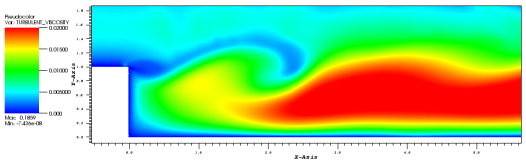

Figure 20: BFS - Optimal μ_t field for KE

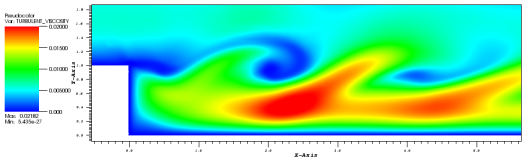

Figure 21: BFS - Optimal μ_t field for EASM

Beyond these observations regarding the best actuation found for the different closures, we propose to compare the characteristics of the corresponding flows. The turbulent viscosity fields are plotted for the best actuations found in Figs. 18 to 21. The optimal configuration found by using the Spalart-Allmaras closure corresponds to a low frequency and large amplitude actuation, which generates a shedding of counter-rotative vortices. For the three other cases, the best actuation found is characterized by a higher frequency, yielding the birth of

smaller vortices at the step corner. The three corresponding flows exhibit similar patterns, although the excitation frequency is different for each case. Especially, the most efficient flows predicted by the SST k-ω and the EASM closures are close to each other. Nevertheless, the non-linearities of the EASM closure generates a more vortical flow, with more intense variations of the turbulent viscosity. The best configuration found by using the Launder-Sharma k-ε closure has a lower actuation frequency. The corresponding flow exhibits vortices with larger span and a far higher turbulent viscosity level. Therefore, some similarities between the flows with optimal actuation are observed, except for the Spalart-Allmaras closure. This seems to indicate that the different optimization exercises yield the same flow characteristics, whatever the closure.

6. INFLUENCE OF ACTUATION PARAMETERS

6.1 Test-case: 25° ramp

The ramp is a backward-facing step with a slope of 25°. This test-case is a configuration chosen by the GDR (Groupement de recherche or Joint Research Project in English) which is a CNRS federative project between French academic research laboratories and ONERA departments working in the framework of flow control. The geometry is represented in Fig. 22.

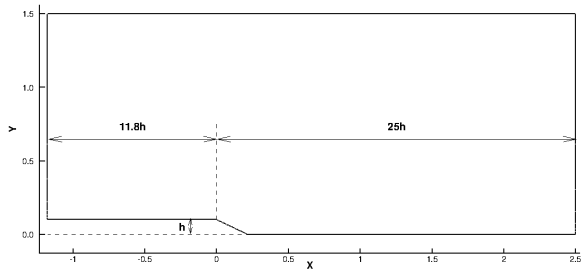

Figure 22: Ramp - Computational domain

The step height h is equal to 100 mm and the slope of the step is equal to 25 degrees. The position of the synthetic jet is located just after the step. The width of the slot is d = 0.5 mm, *i.e.* 0.05h. The inlet of the computational domain is located at 11.8h of the corner of the step and the outlet at 25h. The mesh is generated by Hexpress™, an automatic unstructured mesh generator. This software generates meshes containing only hexahedrons. The mesh contains 73502 nodes and 71375 cells.
At the inlet, a uniform velocity U_∞ = 20 m/s, which corresponds to a Reynolds number of Re= 1.23×10^5 with respect to the height of the ramp, h, is imposed as well as the top of the computational domain. At the outlet, the pressure is imposed. The walls have a no-slip condition and the boundary layer is refined at the wall to fulfill the $y^+ < 0.4$ criterion.

6.2 Results

In this study, the SST $k-\omega$ model is used. Firstly, we consider a configuration without the synthetic jet actuator. This test-case is called non-controlled configuration. Fig. 23 presents a comparison of the velocity profile between the experimental data [12] and the numerical results at X/h = -2.4. We observe a good agreement between the experimental data and the numerical results. This comparison confirms that the inlet is sufficiently far to get the correct boundary layer.

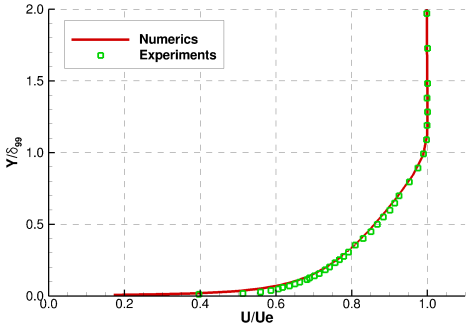

Figure 23: Ramp - Comparison of the velocity profile at X/h = -2.4 for the non-controlled configuration

The streamlines obtained by the numerical results and in experiments are presented in Fig. 24. A massive separation exists and any vortex shedding disappears. The recirculation is characterized by a length called L_R. The numerical simulation predicts L_R/h = 5.333 and in experiments L_R/h = 5.3. The drag coefficient on the ramp is $Cd = F_X/(0.5\rho U_\infty^2 h$ = 0.233.

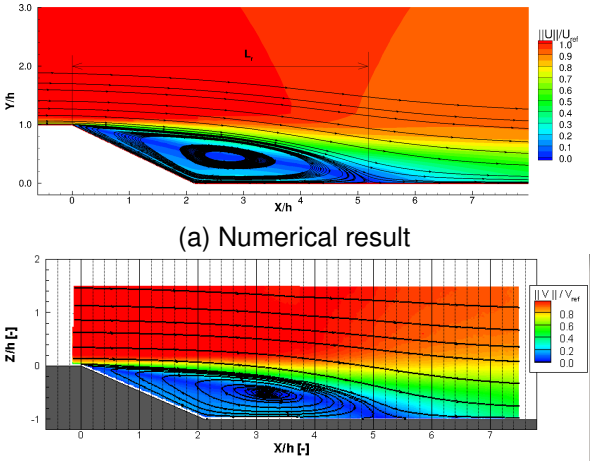

(a) Numerical result

(b) Experimental result

Figure 24: Ramp - Comparison of the velocity profile at X/h = -2.4 for the non-controlled configuration

In the following, we consider the configuration with use of a synthetic jet which will help to modify the flow dynamics. As the main goal is to reduce the recirculation length, the determination of efficient flow control parameters, especially in terms of jet frequency, jet amplitude and injection angle, are important. The period of the synthetic jet, called T_J, is described with 360 time steps and the numerical simulation is carried out with 30 jet periods. The averaged flow is obtained by using the last 10 periods.

In a first time, the optimization of the synthetic jet parameters are restricted to the amplitude and the frequency. To construct the *a priori* database used to explore the design space, the parameters of the synthetic jet are supposed to vary in the following ranges: 5 m/s $\leq U_J \leq$ 150 m/s for the amplitude and 25 Hz $\leq f_J \leq$ 1000 Hz for the frequency. The jet direction is normal to the wall.

The time history of the optimization process is represented in Fig. 25. For each step of optimization, three new features of the synthetic jet (amplitude and frequency) are defined. The best control is obtained at the fifth step. With the amplitude U_J = 136.53 m/s and the frequency f_J = 67.05 Hz, the reattachment point is located at 3.728h. With these features of the synthetic jet, the position of the reattachment point is decreased by 30% approximately. Fig. 26 presents a view of the streamline. The non-dimensional moment coefficient $c_\mu = 2s/h\ U_J^2/U_\infty^2$ = 0.466. With these jet features, the drag coefficient on the ramp is Cd = 0.184, a decrease of 21% compared to the non-controlled configuration.

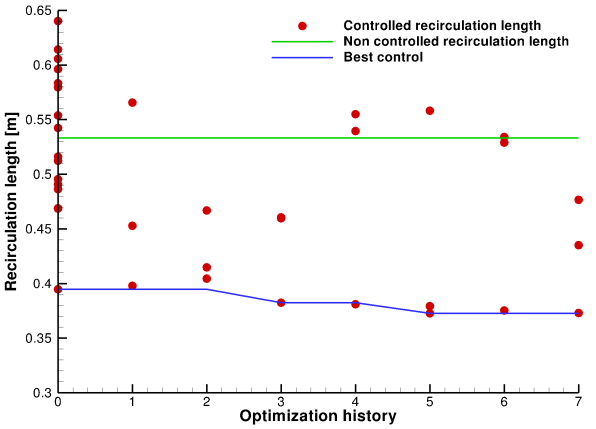

Figure 25: Ramp - Optimization history for the search with two parameters

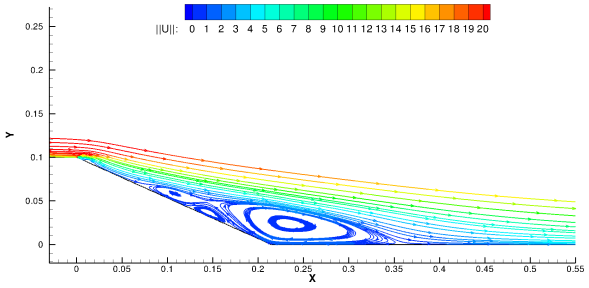

Figure 26: Ramp - Streamlines of the best result for the search with two parameters

In a second phase, the optimization of the jet angle in addition to the amplitude and the frequency is investigated. The parameters of the synthetic jet varies in the following range: 5 m/s $\leq U_J \leq$ 150 m/s for the amplitude and 25 Hz $\leq f_J \leq$ 1000 Hz for the frequency and 0° $\leq d_J \leq$ 180° for the direction of the synthetic jet.

As the previous study, several steps of optimization are used to find the best parameters of the jet. This history is represented in Fig. 27. The best control is obtained at the seventh step. The parameters of the jet are U_J = 124.80 m/s for the amplitude, F_J = 92.00 Hz for the frequency and d_J = 27.00° for the direction. With these parameters, the reattachment point is located at 2.622h, a decrease of 51%. The non-dimensional moment coefficient is 0.389. The averaged flow is presented in Fig. 28. The drag coefficient on the ramp is Cd = 0.074, a decrease of 68% compared to the non-controlled configuration.

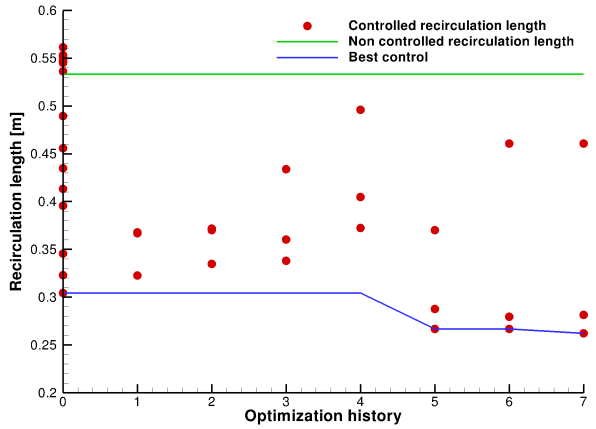

Figure 27: Ramp - Optimization history for the search with three parameters

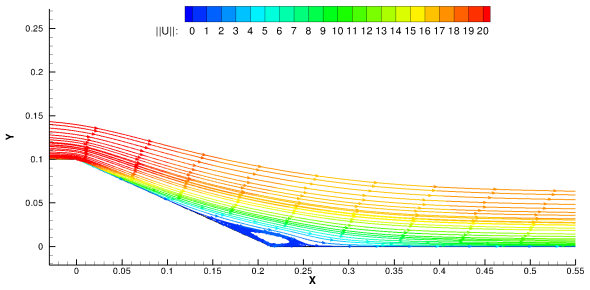

Figure 28: Ramp - Streamlines of the best result for the search with three parameters

7. CONCLUSION AND PROSPECTS

The optimization of a flow control device has been carried out, by coupling a URANS model with a statistical learning method. Three different test-cases have been studied: lift enhancement for the NACA 0015 airfoil, separation length reduction for a backward facing step and a 25° ramp.

As illustrated, this approach allows to account for truncated simulations and related errors in a rigorous and systematic statistical framework. However, the optimization of control devices remains a numerical challenge. The influence of the turbulence closure has been quantified. Although discrepancies have been noted, some similarities between the flow patterns obtained using different closures have been reported. Finally, a significant impact of the choice of actuation parameters has been observed. In particular, the jet direction appeared to be a critical parameter for the efficiency of the control.

Forthcoming works will imply a larger number of devices, with application to three-dimensional flow problems. A second research axes will study how to account for operational condition uncertainty in such an approach.

References

[1] DRIVER, D., AND SEEGMILLER, H. Features of a reattaching turbulent shear layer in divergent channel flow. *AIAA journal 23*, 2 (1985), 163–171.

[2] DUVIGNEAU, R., AND CHANDRASHEKAR, P. Kriging-based optimization applied to flow control. *Int. J. for Numerical Methods in Fluids 69*, 11 (2012), 1701–1714.

[3] DUVIGNEAU, R., HAY, A., AND VISONNEAU, M. Optimal location of a synthetic jet on an airfoil for stall control. *Journal of Fluid Engineering 129*, 7 (July 2007), 825–833.

[4] DUVIGNEAU, R., AND VISONNEAU, M. Optimization of a synthetic jet actuator for aerodynamic stall control. *Computers and Fluids 35* (July 2006), 624–638.

[5] DUVIGNEAU, R., VISONNEAU, M., AND DENG, G. B. On the role played by turbulence closures in hull ship optimization at model and full scale. *Journal of Marine Science and Technology 8* (2003), 11–25.

[6] EL-HACK, M. G., POLLARD, A., AND BONNET, J.-P. *Flow control: fundamentals and practices*. Springer-Verlag, 1998.

[7] GARNIER, E., PAMART, P., DANDOIS, J., AND SAGAUT, P. Evaluation of the unsteady rans capabilities for separated flow control. *Computers & Fluids 61* (2012), 39–45.

[8] GUILMINEAU, E., DENG, G. B., AND WACKERS, J. Numerical simulation with a DES approach for automotive flows. *Journal of Fluids and Structures 27* (2011), 807–816.

[9] JONES, D. Efficient global optimization of expensive black-box functions. *Journal of Global Optimization 13*, 4 (1998).

[10] LABROQUÈRE, J., DUVIGNEAU, R., AND GUILMINEAU, E. Impact of turbulence closures and numerical errors for the optimization of flow control devices. In *21th AIAA Computational Fluid Dynamics Conference, San Diego, USA* (2013).

[11] RUMSEY, C. L., GATSKI, T. B., SELLERS, W. L., VATSA, V. N., AND VIKEN, S. A. Summary of the 2004 Computational Fluid Dynamics Validation Workshop on synthetic jets. *AIAA Journal 44*, 2 (2006), 194–207.

[12] THACKER, A., AND JOUSSOT, R. Présentation des premiers résultats expérimentaux sur le montage du gdr. Réunion du GDR Contrôle des décollements, juin 2012.

[13] WACKERS, J., DENG, G. B., GUILMINEAU, E., LEROYER, A., QUEUTEY, P., AND VISONNEAU, M. Combined refinement criteria for anisotropic grid refinement in free-surface flow simulation. *Computers & Fluids 92* (2014), 209–222.